Human Molecular Genetics, 2005, Vol. 14, No. 5 ***565–574***
doi:10.1093/hmg/ddi053
Advance Access published on January 13, 2005

The R6/2 transgenic mouse model of Huntington's disease develops diabetes due to deficient β-cell mass and exocytosis

Maria Björkqvist[1,*], Malin Fex[1], Erik Renström[2], Nils Wierup[3], Åsa Petersén[4], Joana Gil[4], Karl Bacos[1], Natalija Popovic[4], Jia-Yi Li[4], Frank Sundler[3], Patrik Brundin[4] and Hindrik Mulder[1]

[1]Department of Cell and Molecular Biology, BMC C11, 221 84 Lund, Sweden, [2]Department of Physiological Sciences, The Diabetes Programme at Lund University, BMC B11, SE-211 84 Lund, Sweden, [3]Section for Neuroendocrine and Cell Biology BMC F10, 221 84 Lund, Sweden and [4]Section for Neuronal Survival, BMC A10, 221 84 Lund, Sweden

Received September 15, 2004; Revised December 15, 2004; Accepted January 4, 2005

Diabetes frequently develops in Huntington's disease (HD) patients and in transgenic mouse models of HD such as the R6/2 mouse. The underlying mechanisms have not been clarified. Elucidating the pathogenesis of diabetes in HD would improve our understanding of the molecular mechanisms involved in HD neuropathology. With this aim, we examined our colony of R6/2 mice with respect to glucose homeostasis and islet function. At week 12, corresponding to end-stage HD, R6/2 mice were hyperglycemic and hypoinsulinemic and failed to release insulin in an intravenous glucose tolerance test. *In vitro*, basal and glucose-stimulated insulin secretion was markedly reduced. Islet nuclear huntingtin inclusions increased dramatically over time, predominantly in β-cells. β-cell mass failed to increase normally with age in R6/2 mice. Hence, at week 12, β-cell mass and pancreatic insulin content in R6/2 mice were 35 ± 5 and 16 ± 3% of that in wild-type mice, respectively. The normally occurring replicating cells were largely absent in R6/2 islets, while no abnormal cell death could be detected. Single cell patch-clamp experiments revealed unaltered electrical activity in R6/2 β-cells. However, exocytosis was virtually abolished in β- but not in α-cells. The blunting of exocytosis could be attributed to a 96% reduction in the number of insulin-containing secretory vesicles. Thus, diabetes in R6/2 mice is caused by a combination of deficient β-cell mass and disrupted exocytosis.

INTRODUCTION

Huntington's disease (HD) is a fatal autosomal dominant neurodegenerative disease. The prevalence of HD is four to seven in 100 000 and it typically develops in mid-life. The symptoms involve psychiatric, motor and cognitive disturbances, and weight loss. In addition, there is an increased incidence of diabetes mellitus in HD patients. Ten to 25% of HD patients exhibit impaired glucose homeostasis (1). Reductions in both insulin sensitivity and secretion are apparent.

HD is caused by an expansion of a CAG repeat in *exon* 1 of the *huntingtin* gene (2), which encodes a protein suggested to be associated with synaptic vesicles and microtubules in neurons (3,4). There is evidence that huntingtin directly and/or indirectly plays a role in vesicle trafficking and neurotransmission (5). It has also been shown that normal huntingtin is anti-apoptotic in brain cells (6–8) and protects from toxicity induced by the mutant protein (9,10).

A common feature of mutant huntingtin and other mutant proteins involved in CAG-repeat expansion diseases is a tendency to form insoluble aggregates that accumulate in the cytoplasm and nucleus of cells (11). In HD patients, intranuclear inclusions have been described in the striatum and cortex (12,13), whereas in mouse models of the disease inclusions appear to be more widely distributed and have been demonstrated also in peripheral tissues (14). Huntingtin depositions are viewed by many as key players in the pathogenetic process in basal ganglia neurons in HD (13,15). The mechanisms, however, whereby striatal and cortical neurons die in HD have not been resolved. Impaired energy metabolism (16), excitotoxicity (17) and oxidative stress (18) have been implicated. Huntingtin is expressed not only in neurons, but also in several other tissues

*To whom correspondence should be addressed at: Department of Cell and Molecular Biology, Section for Molecular Signaling, Lund University, BMC C11, SE-221 84 Lund, Sweden. Email: maria.bjorkqvist@medkem.lu.se

including endocrine tissues such as pancreatic islets (19). Therefore, if the same fundamental cellular pathology, presumably caused by mutant huntingtin, occurs also in pancreatic β-cells, it may explain why β-cells become dysfunctional in HD patients and diabetes subsequently evolves. Conversely, examining this assumed fundamental cellular dysfunction may shed new light on the pathological processes occurring in neurons.

To facilitate the study of HD pathogenesis, several transgenic mouse models of HD have been created (20). The first model was the R6/2 mouse (21), which expresses *exon 1* of the human *HD* gene, containing 150 CAG repeats. Consequently, the mice develop neurological symptoms that resemble many of those seen in HD. These include deficits of motor co-ordination, altered locomotor activity, impaired cognitive performance and seizures. Specific behavioral tests detect cognitive symptoms already around week 3–4 (22), whereas motor symptoms typically develop later. In most breeding colonies, the R6/2 mice die at week 12–14 for unknown reasons. At this stage, there is significant atrophy of the striatum and neocortex and widespread occurrence of neuronal intranuclear inclusions of mutant huntingtin. Although we recently demonstrated loss of a specific population of orexin-expressing neurons in the hypothalamus of R6/2 mice and HD patients (23), surprisingly little evidence for cell death in the brain of R6/2 mice has emerged (13,24–26).

The R6/2 mice also exhibit pathological changes in tissues outside the central nervous system (27,28). For instance, huntingtin inclusions appear in skeletal and cardiac muscles, medullary cells in the adrenal gland, hepatocytes and pancreatic islets (14). With respect to pancreatic islets, the inclusions may be involved in the development of hyperglycemia and insulin-deficient diabetes in R6/2 mice (27,29). Whether the reduced levels of islet and circulating insulin are associated with reduced β-cell mass has not been determined (29). It has been proposed that R6/2 mice develop diabetes due to interference with transcriptional regulation in islets (13,29). This has been suggested to be caused by the insoluble nuclear protein aggregates containing huntingtin. The fact that misfolded huntingtin forms intranuclear inclusions also in pancreatic β-cells (13,29) suggests that pathological changes in β-cells have features in common with those that take place in the nervous system in HD. Thus, unraveling these processes may also shed light on pathological processes in the brain of R6/2 mice. Moreover, glucose homeostasis and islet function may be readily accessible parameters that can be monitored as measures of the progress of HD and to assess the effects of possible therapeutic interventions effective also in the brain. For these reasons, we set out to elucidate the pathogenetic mechanisms underlying diabetes in R6/2 mice. We found that dual events lead to the development of diabetes in the R6/2 mice: (1) replication of β-cells was impaired in R6/2 islets, resulting in deficient β-cell mass, and (2) β-cells exhibited a dramatically decreased number of insulin-containing secretory vesicles accounting for an abolishment of exocytosis.

RESULTS

Expression of huntingtin in pancreatic islets

Nuclear inclusions presumably derived from huntingtin have previously been demonstrated in islets from R6/2 mice (14). However, expression of the native protein in islets has not been described. To study this, islets were isolated from wild-type mice, untreated Sprague-Dawley rats and clonal insulin-producing cells (832/13 cells), and analyzed with RT–PCR. As shown in Figure 1A, huntingtin mRNA was present in rodent islets as well as clonal β-cells. The presence of huntingtin protein in the clonal β-cells and islets was confirmed by western blotting (data not shown).

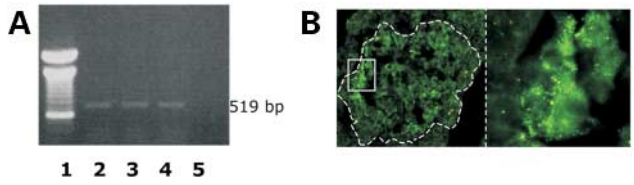

Figure 1. Huntingtin is expressed in pancreatic islets. (**A**) Ethidium bromide-stained agarose gel showing products of RT–PCR generated with specific primers for a 519 bp fragment of huntingtin in rat islets (2), mouse islets (3) and clonal insulin cells (832/13 cells) (4). Lane 5 is a negative control (DEPC water). Distribution of wild-type huntingtin in rat pancreatic islets. (**B**) A granular immunoflourescence occurs in the majority of islet cells, suggesting that mainly β-cells, but also other islet cell-types express huntingtin. Dashed line indicates the islet. The right panel is a blow-up of the inserted box in the left panel.

To elucidate cellular expression of huntingtin in the pancreas, immunocytochemistry was performed. However, because only a monoclonal antibody to huntingtin was at our disposal, immunocytochemistry for this antigen in mouse pancreatic sections was technically not possible, due to the binding of the mouse secondary antibody to immunoglobulins in the tissue. Instead, to attain some information on cellular localization of huntingtin in rodent islets, we performed experiments in rat pancreatic sections (Fig. 1B); here, the majority of islet cells expressed huntingtin, implying that β-cells account for the larger part of huntingtin expression in islets.

Nuclear inclusions in pancreatic islets

The pathology in HD patients and R6/2 mice may be associated with the formation of nuclear inclusions derived from the mutant huntingtin. Therefore, we examined whether islet cells in our colony of R6/2 mice also exhibit the nuclear inclusions typical of HD (13). Double immunocytochemistry in pancreatic sections, using antibodies to insulin and an antibody to the mutant huntingtin protein, showed that islets in wild-type mice lacked huntingtin inclusions (Fig. 2A). In R6/2 mice, however, inclusions could be seen in the nuclei of 19% (86 cells out of 450, three different mice) of β-cells already at week 7 (Fig. 2B); at week 12, the frequency of the inclusions increased dramatically and occurred in a majority (>95%) of the β-cells (Fig. 2C). Huntingtin inclusions could not be detected either in glucagon-producing α-cells or in somatostatin-producing δ-cells at 7 weeks, although at 12 weeks, 24% (51/212 cells, three different mice) of the α-cells and 6% (6/97 cells, four different mice) of the δ-cells contained inclusions. Clearly, the β-cell is more prone to huntingtin deposition than the neighboring islet cell types.

Metabolic characterization of the R6/2 mice

Body weight was similar in R6/2 and wild-type mice up to 10 weeks of age after which it declined in R6/2 mice (data

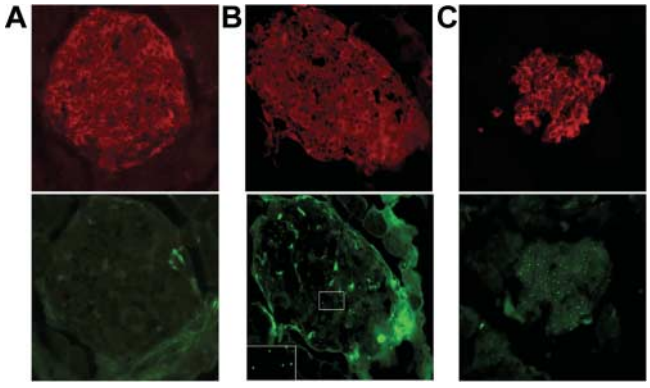

Figure 2. Distribution of huntingtin inclusions in pancreatic islets. (**A**) Pancreatic islet from a 12-week-old wild-type mouse double immunolabeled for insulin (top panel) and for huntingtin inclusions (EM48; lower panel). (**B**) Pancreatic islet from a 7-week-old R6/2 mouse double immunolabeled for insulin (top panel) and huntingtin inclusions (lower panel). (**C**) Pancreatic islet from a 12-week-old R6/2 mouse double immunolabeled for insulin (top panel) and huntingtin inclusions (lower panel). The frequency of nuclear inclusions, seen as punctate immunofluorescent pinheads, increased with age in R6/2 mice but were lacking in wild-type mice.

not shown). Plasma glucose levels rose progressively in R6/2 mice compared with wild-type mice and at 12 weeks, the majority of mice were hyperglycemic (Fig. 3). Serum glucose was 19.6 ± 1.59 versus 12.3 ± 0.84 mM in wild-type mice ($n = 10$, $P < 0.001$). Circulating insulin levels gradually decreased over time in R6/2 mice. In 12-week-old R6/2 mice, serum insulin was 0.89 ± 0.21 versus 1.45 ± 0.32 ng/ml in wild-type mice ($n = 10$, $P = 0.002$).

Glucose tolerance test

To further examine glucose homeostasis, the mice were subjected to a glucose tolerance test at week 11.5. Glucose disposal was retarded in the R6/2 mice (Fig. 4A); the area under curve (AUC) was increased by 25% ($P = 0.035$). Remarkably, during the test, the insulin response was virtually absent (Fig. 4B); AUC for R6/2 mice was 66% of that in wild-type mice ($P = 0.015$). Together with the increase in basal plasma glucose and reduced circulating insulin levels, the results demonstrate that R6/2 mice develop insulin-deficient diabetes.

Insulin secretion *in vitro*

To further clarify the secretory deficiency observed *in vivo*, we examined insulin secretion *in vitro* in islets isolated from the mice. At week 7, insulin secretion from R6/2 islets was similar to that from wild-type islets in response to both 2.8 and 16.7 mM glucose (Fig. 5A). In contrast, at week 12, insulin secretion in response to both 2.8 and 16.7 mM glucose was reduced 4-fold ($P < 0.001$) in the islets from the R6/2 mice compared with wild-type islets (Fig. 5B). We also examined insulin secretion in response to 35 mM KCl. KCl depolarizes the β-cell and provokes insulin secretion, which is a measure of β-cell function independent of metabolic regulation. Again, insulin secretion from R6/2 islets

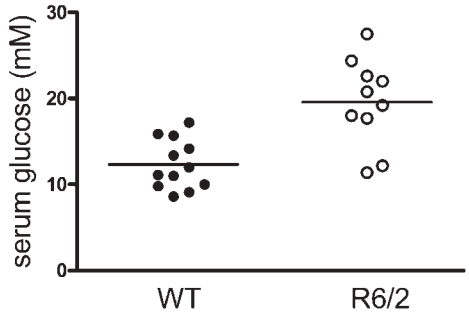

Figure 3. Plasma glucose in 12-week-old wild-type and R6/2 mice. Plasma glucose was 19.6 ± 1.59 versus 12.3 ± 0.84 mM in wild-type mice ($n = 10$, $P < 0.001$).

was impaired compared with that from wild-type islets at 12 week (2.5-fold reduction, $P = 0.012$; Fig. 5B).

Morphological and immunochemical characterization of islets

Pancreatic sections from R6/2 and wild-type mice were immunostained for insulin. At week 7, the appearance and size of β-cell mass in the two genotypes were indistinguishable. In contrast, at week 12, islets in R6/2 mice appeared hypotrophic compared with the wild-type mice (Fig. 2).

To quantify the apparent reduction in β-cell mass, an unbiased analysis using stereological morphometry was performed in sections immunostained for insulin and prepared for light microscopy. Thus, confirming the observations from immunofluorescence for insulin, there was no difference in β-cell mass at week 7, as reflected by the surface area in the sections covered by β-cells. However, at week 12, insulin-immunostained area in pancreatic sections from R6/2 mice was 55% of that in wild-type mice ($P < 0.0001$) (Fig. 6). Islet number was unaffected at both time points (data not shown).

At week 7, insulin content in islets was similar in both genotypes. In contrast, at week 12, there was a significant reduction in insulin content in islets from R6/2 mice (Table 2). Furthermore, tissue content of the islet hormones was measured. As shown in Table 1, there was a dramatic decrease in pancreatic insulin content as well as somatostatin content in 12-week-old R6/2 mice, whereas glucagon content remained unchanged.

FluoroJade-staining and evaluation of neogenesis/regeneration

FluoroJade (FJ) stains dying cells in the brain as well as in other tissues (30). This stain revealed no signs of cell death at either 7 or 12 weeks (data not shown). Another potential explanation for the deficient β-cell mass in R6/2 mice is a reduction in neogenesis and/or regeneration of islet cells. These events require replication of cells and therefore, we injected mice systemically with the nucleotide analog bromodeoxyuridine (BrdU) and examined its incorporation into nuclei of dividing cells. Remarkably, there was a 6-fold reduction in BrdU-positive cells/islet in R6/2 compared with

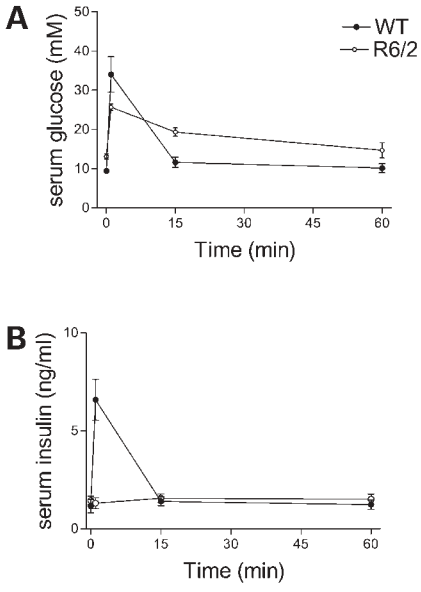

Figure 4. Glucose tolerance test conducted in 11.5-week-old mice. Intravenous glucose (1 g/kg) was given at time point 0 and plasma glucose (**A**) and plasma insulin (**B**) were determined at 0, 5, 15 and 60 min ($n = 6–11$).

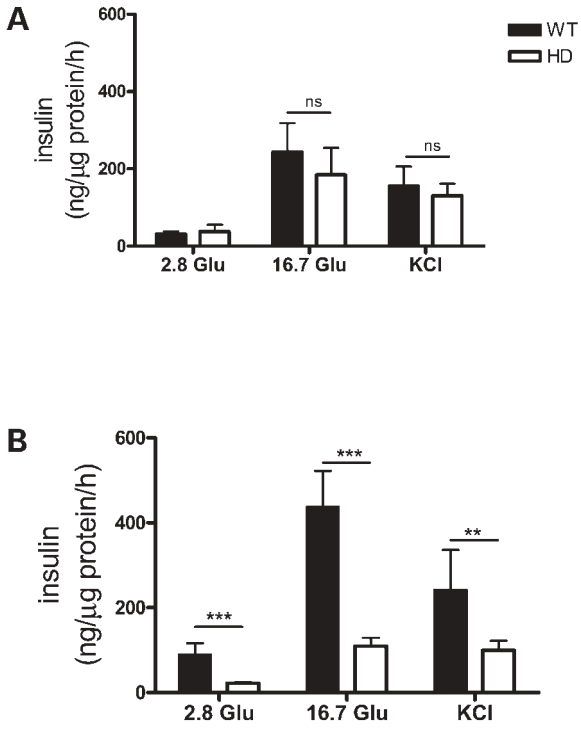

Figure 5. Insulin secretion from isolated pancreatic islets. (**A**) 7-week-old mice and (**B**) 12-week-old mice. Insulin secretion was stimulated by 2.8 mM glucose (basal), 16.7 mM glucose or 35 mM KCl. Means ± SEM; $n = 6$. Student's t-test was used to assess difference between the two groups. $^{***}P < 0.001$; $^{**}P < 0.01$; ns, not significant.

wild-type mice (Fig. 7), implying that replication of islet cells is impaired.

Cell death at an ultrastructural level

At this point, cell death had been examined by markers at the light and fluorescence microscopic level. To extend this work, we examined the islets at the ultrastructural level, to see whether any signs of apoptosis or necrosis could be identified. Confirming our observations using morphometry, the islets in 12-week-old R6/2 mice were considerably smaller as assessed by electron microscopy. While α- and δ-cells appeared normal in appearance and frequency, the number of β-cells was dramatically reduced. Despite this reduction, no signs of apoptosis (e.g. membrane blebbing, pyknotic nuclei) or necrosis were observed (Fig. 8). This agrees with our findings at the light microscopic level and suggests that an impairment of replication, as opposed to cell death, is the cause of the observed reduction in β-cell mass in R6/2 mice.

Age-dependent effects on single-cell exocytosis of insulin and glucagon in R6/2 mice

We next characterized the secretory defect observed in R6/2 mice at the level of the single β-cell (Fig. 9). Exocytosis was measured as increases in cell capacitance (ΔC) and was evoked by trains of ten 500 ms voltage-clamp depolarizations that activated the endogenous voltage-gated Ca^{2+} channels. In control β-cells, such stimulation evoked an average 430 ± 15 fF capacitance increase ($n = 13$; Fig. 9A). When analyzing the amplitude of exocytosis evoked by the respective pulses of the train stimulus (Fig. 9B), the exocytotic response to the first depolarization was the largest (108 ± 8 fF) and then decreased during the train stimulus. This pattern of exocytosis is consistent with the view that the β-cell possesses a pool of immediately releasable insulin granules that is emptied within ~1 s after elevation of cytosolic Ca^{2+} (32). When R6/2 mice were examined at 8 weeks of age, insulin exocytosis remained largely intact and overall responses averaged 415 ± 11 fF ($n = 11$; Fig. 9C). Interestingly, closer inspection of the responses to the individual pulses in the train stimulation revealed that the first depolarization evoked a mere 24 ± 7 fF ΔC ($P < 6.22748 \times 10^{-9}$ versus exocytosis evoked by the first pulse in control β-cells) and that substantial exocytosis was not evoked until the third depolarization. This disturbance in exocytotic kinetics is reminiscent of the 'uncoupled' type of exocytosis observed in β-cells in which the physical association between the L-type $Ca_V1.2$ channels and the insulin granules has been disrupted (32,33). This suggests that the insulin exocytotic apparatus is not optimally functional in 8-week-old R6/2 mice. Indeed, when β-cells were isolated from 12-week-old R6/2 mice, depolarization-evoked exocytosis was virtually abolished (total 33 ± 2 fF, $n = 7$; $P < 1.55356 \times 10^{-13}$ versus exocytosis in control mice and $P < 8.8325 \times 10^{-15}$ versus 8-week-old R6/2 mice). It was ascertained that these effects on exocytosis occurred without any noticeable change in train depolarization-associated Ca^{2+} influx. In addition, after the train stimulation, Ca^{2+} current–voltage relations were investigated in all cells over the voltage range −50 to +50 mV. Maximal Ca^{2+} influx was invariably observed at 0 mV and averaged 74 ± 12, 82 ± 9 and 85 ± 14 pA at this potential in β-cells from control, 8- and 12-week-old R6/2 mice, respectively (data not shown).

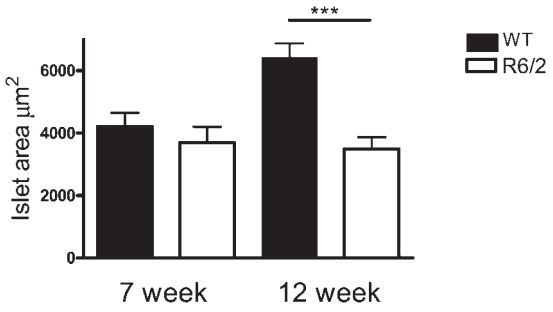

Figure 6. Insulin-immunostained area in islets from 7- and 12-week-old mice. Means ± SEM were given. Two-factor ANOVA was used to assess difference between the two groups. $^{***}P < 0.001$.

We next measured glucagon exocytosis evoked by train depolarizations in single α-cells from R6/2 mice (Fig. 10). Depolarization-evoked glucagon exocytosis was on average more intense than in the β-cells, in excellent agreement with previous observations (34). In control α-cells, a train depolarization evoked a 950 ± 47 fF increase in cell capacitance ($n = 4$), which remained largely intact also in the R6/2 α-cells (770 ± 33 and 700 ± 82 fF, $n = 7$ and 3, in 8- and 12-week-old R6/2 α-cells, respectively).

Ultrastructural β-cell appearance

A possible explanation for the disruption of exocytosis is depletion of secretory vesicles. To explore this possibility, islets were examined at the ultrastructural level. Indeed, β-cells from 12-week-old R6/2 mice contained very few insulin secretory vesicles (7 ± 1.5 compared with wild-type 171 ± 12.5 $n = 10$; Fig 8). This finding agrees with our determination of islet content of insulin (Table 2), which was relatively lower than β-cell mass (16 ± 3 versus 35 ± 5%), thus indicating that deficient β-cell mass alone cannot account for the reduction of islet insulin content.

DISCUSSION

Neurodegenerative disorders are associated with endocrine abnormalities (35,36). Several studies show a high prevalence of glucose intolerance and diabetes in patients with Alzheimer's disease, Parkinson's disease, Friedreich's ataxia and HD (1,37,38). Importantly, it has been shown that perturbed glucose homeostasis and frank diabetes occur with a variable penetrance in R6/2 mice (26–28).

Diabetes is not restricted to one type of transgenic HD mice. Hyperglycemia has also been observed in the HD-N171-82Q mouse (39). This suggests that the endocrine pathology is an important feature of the polyglutamine disease. Indeed, the pathogenetic mechanisms in the pancreatic islets of the mouse models may be relevant to the changes in glucose homeostasis observed in HD patients. In addition, they could also reflect important cellular changes that occur in neurons and that contribute to the neurological symptoms. Therefore, a deeper understanding of why the pancreatic islets fail in transgenic mouse models of HD could ultimately lead to the discovery of novel therapeutic targets in the brain.

Table 1. Insulin, glucagon and somatostatin content in pancreatic extracts from 12-week-old wild-type and R6/2 mice (mean ± SEM were given; Student's *t*-test was used to assess difference between the two groups)

Genotype	Insulin (ng/mg)	Glucagon (ng/mg)	Somatostatin (ng/mg)
WT	110.5 ± 6.5 $n = 8$	3.21 ± 0.47 $n = 8$	291 ± 34.1 $n = 6$
R6/2	17.3 ± 4.2* $n = 6$	2.55 ± 0.64 $n = 6$	31.2 ± 4.9* $n = 6$

*$P < 0.001$.

In our studies of R6/2 mice, plasma glucose levels increased over time. Moreover, in the glucose tolerance test at week 12, glucose disposal was markedly retarded and the ability of glucose to provoke insulin secretion virtually absent. Insulin secretion and content in islets were unaffected at week 7 in R6/2 mice compared to wild-type mice. At week 12, insulin content was increased in the wild-type mice, whereas it was decreased in the R6/2 mice. Concomitantly, both basal secretion and glucose-stimulated insulin secretion were impaired at week 12. These observations were further substantiated by morphometric analysis of islets. Again, at week 7, islet number and β-cell mass were similar in both genotypes. In wild-type mice, β-cell mass was doubled when the mice reached the age of 12 weeks. In contrast, R6/2 islets did not increase in size. Clearly, the insulin secretory deficiency in R6/2 islets is paralleled by a deficiency in β-cell mass and insulin content, suggesting a casual relationship.

Previous reports have described reductions in pancreatic levels of glucagon, insulin and insulin mRNA in R6/2 mice (26,28); islet appearance in these studies was described as normal. In our study, we do not observe a marked reduction in the pancreatic level of glucagon. In fact, α-cells do not appear to be affected to the same extent as β-cells by nuclear inclusions of huntingtin (α-cells in the 12-week-old R6/2 mouse display intranuclear inclusions to the same extent as β-cells at week 7), despite the fact that α- and β-cells share common endocrine features as well as embryonic background (40). The observed reduction in somatostatin levels could be a compensatory mechanism, due to low levels of insulin; the foremost function of somatostatin in islets is as a paracrine inhibitor of insulin release (41). δ-cells were virtually unaffected by huntingtin inclusions and our preliminary studies suggest that the number of δ-cells is unchanged (data not shown).

We examined the underlying cause of the reduction in β-cell mass in R6/2 mice by using markers for cell death and replication as well as ultrastructural studies by electron microscopy. Surprisingly, there were no indications of increased cell death in islets. Instead, a marked decrease in the replication of β-cells was observed. This implies that neogenesis and/or regeneration of islet cells is impaired. Although the replication rate of β-cells is normally low (42), a reduction will ultimately result in reduced β-cell mass and could explain the reduction in β-cell mass in R6/2 mice. We have recently shown that there is a significant reduction in cell proliferation in the hippocampus of 12-week-old R6/2 mice compared with their wild-type littermates (43). Another group has reported an impairment of hippocampal cell proliferation in the R6/1 HD mouse model (44). A failure of proliferation of fibroblasts derived from 12-week-old R6/2 mice has also

Table 2. Insulin content in isolated islets from 7- and 12-week-old wild-type and R6/2 mice (means ± SEM were given; two-factor ANOVA was used to assess difference between the two groups)

Genotype	Insulin 7 W (ng/μg protein)	Insulin 12 W (ng/μg protein)
WT	448 ± 93	780 ± 218
R6/2	388 ± 76	201 ± 71*

*$P < 0.001$.

been reported (45). These findings together suggest a generalized impairment of cell replication, which could play an important pathogenic role in various tissues in R6/2 mice. It could provide an explanation for the reduced cell number and atrophy found in some brain regions in R6/2 mice, while signs of cell death have been more difficult to identify (13,22–25).

Despite the striking deficiency of β-cell mass (∼35% reduction), this in itself may not be sufficient to provoke diabetes in the mouse (46). For this reason, we also tried to identify a functional impairment of β-cells in R6/2 mice. We found that the electrical activity in R6/2 β-cells was intact. In contrast, exocytosis induced by membrane depolarization was abolished in β-cells from 12-week-old R6/2 mice. This agrees with the dramatic reduction in the number of secretory vesicles in R6/2 β-cells, as observed by electron microscopy, raising the possibility of a specific perturbation of the exocytotic process in these cells. Indeed, exocytosis in α-cells was unaffected. This agrees with the finding that nuclear inclusions of huntingtin appeared to a lesser extent in α-cells; consequently, the ultrastructural appearance of these cells was unchanged. In fact, perturbations of exocytosis have been demonstrated in *in vitro* models of HD, e.g. impaired expression of the exocytotic protein complexin II in PC12 cells expressing mutant huntingtin (47). In these experiments, however, reduced numbers of granules were not reported.

In conclusion, we have identified two separate pathological processes that are responsible for diabetes in R6/2 mice: impaired β-cell replication, resulting in deficient β-cell mass, and a loss of insulin-containing secretory granules, abrogating stimulated hormone secretion. As discussed, previous reports have described similar impairments in experimental models of HD (47). This highlights the importance of elucidating pathologies in endocrine cell systems in HD. Resolving the pathogenic and molecular events leading to β-cell loss and β-cell dysfunction could potentially contribute to the understanding of neurological symptoms in HD and the fundamental pathogenesis of the disease. Such efforts may also generate tools for improved monitoration and treatment of this devastating disease.

MATERIALS AND METHODS

Animals and plasma analyses

The colony of R6/2 mice has been previously described in detail (43,48). For the present experiments, male and female littermate heterozygote R6/2 and wild-type mice were used. Blood was obtained by retro-orbital bleeding from anesthetized mice [midazolam 0.4 mg/mouse (Dormicum®, Hoffman-La-Roche, Basel, Switzerland) and a combination of fluanison (0.9 mg/mouse) and fentanyl (0.02 mg/mouse; Hypnorm®, Janssen, Beerse, Belgium)]. Glucose was measured using the glucose oxidase method (Thermo Trace, Victoria, Australia). Plasma insulin levels were determined by radioimmunoassay (RIA; Linco Research Inc., St. Louis, MO, USA). The experiments were approved by the Regional Animal Ethics Committee in Lund.

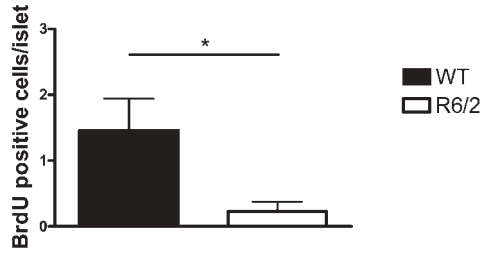

Figure 7. BrdU-positive cells in islets from 7-week-old wild-type and R6/2 mice. Means ± SEM were given. Student's *t*-test was used to assess difference between the two groups. *$P < 0.05$.

R6/2 mice in the terminal phase, where neurological symptoms have evolved, have difficulties to procure any food. For this reason, it was unethical and harmful to the mice to subject them to blood sampling under fasting conditions, which would have demonstrated an even more exaggerated metabolic difference between mutant and wild-type mice.

Glucose tolerance test

For the intravenous glucose tolerance test, D-glucose (1 mg/g) was injected into the tail vein of anesthetized mice (see previous subsection). Plasma glucose and insulin levels were determined, as described previously, in retro-orbital blood samples collected at the indicated time points.

Isolation and batch incubation of islets

Islets were isolated by standard collagenase digestion and handpicked under a stereo microscope. Batches of three islets for each condition were kept in HEPES balanced salt solution (HBSS; 114 mM NaCl, 4.7 mM KCl, 1.2 mM KH_2PO_4, 1.16 mM $MgSO_4$, 20 mM HEPES, 2.5 mM $CaCl_2$, 25.5 mM $NaHCO_3$, 0.2% BSA; pH 7.2) containing 2.8 mM glucose for 60 min in an incubator at 37°C. Then, three islets at a time were transferred to a 96-well plate kept on ice and containing 200 μl per well of the same buffer but with the addition of the respective secretagogue. Following transfer of all islets, the plate was again placed in an incubator at 37°C. At 60 min, a sample from the buffer was removed for the measurement of insulin by RIA (Linco Research Inc.). Islet content of insulin was measured after acid/ethanol extraction.

Reverse transcriptase–PCR analysis

mRNA was isolated from rat isolated islets, mouse isolated islets and clonal insulinoma cells (832/13 cells) (49). The reverse transcriptase (RT) reaction was performed using Superscript preamplification system (Life Technologies,

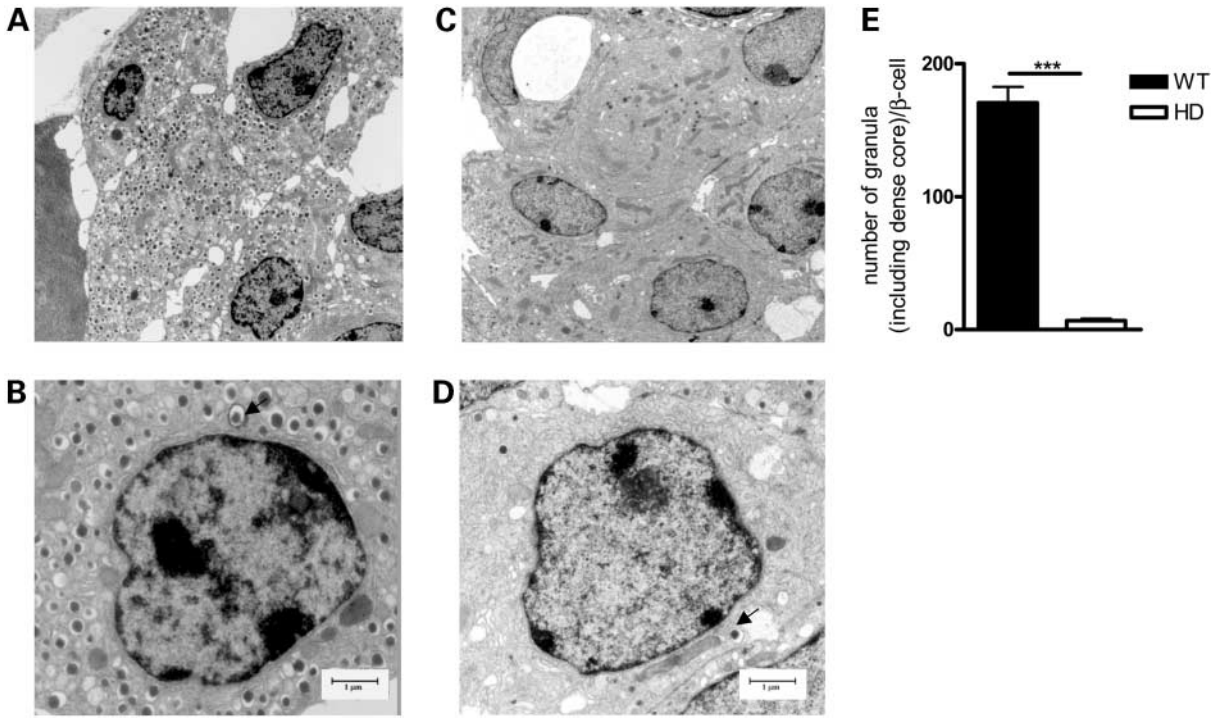

Figure 8. Electron micrographs of β-cells (overview and close up). Wild-type (**A** and **B**) and R6/2 mouse (**C** and **D**). Note lack of secretory granules in β-cells from the R6/2 mouse. Black arrow indicates the characteristic β-cell granules. (**E**) Numbers of dense core granules in the β-cells of wild-type and R6/2 mice. Means ± SEM; 15 cells in each group of consisting of three mice were analyzed. Student's *t*-test was used to assess difference between the two groups. $^{***}P < 0.001$.

New York, NY, USA) according to the manufacturers protocol. The synthesized first-strand cDNA reactions were stored at −80°C. A 1 μl of the cDNA-containing solution was used for the PCR reaction (reaction volume 20 μl) in 10 × PCR buffer containing 1.5 mM $MgCl_2$, 200 μM dNTP and 1 unit Taq enzyme (PCR reagents were purchased from Promega, Madison, WI, USA) with specific primers towards a 519 bp long fragment of mouse huntingtin. The primers for the detection of huntingtin cDNAs were 5′-TCGTACC ACCATTTGTTTTTCA-3 and 5 -CCTTTGGCCTATGAGA TCTGGATGTG-3 . Amplification was performed under the following conditions: denaturation at 94°C for 1 min, annealing at 56°C for 1 min and extension at 72°C for 2 min for a total 45 cycles.

Immunocytochemistry and morphometry

Pancreatic tissue was prepared for immunocytochemistry as previously described (50) and sections were cut on a cryostat (10 μm). An affinity-purified rabbit antibody to insulin (diluted 1:1280; code 9003; Euro-Diagnostica, Malmö, Sweden), a mouse anti-huntingtin protein monoclonal antibody (diluted 1:500, MAB 2166) and a mouse polyclonal antibody recognizing huntingtin inclusions (EM48 1:400 Chemicon International, Temecula, CA, USA) were used for indirect immunofluorescence, as previously described (50).

FJ (Histo Chem, Jefferson, AR, USA) has been shown to stain dying neurons in the brain (30,48) as well as other dying cells (31). Briefly, 10 μm sections were treated with 0.06% potassium permanganate in H_2O for 15 min and washed twice in H_2O and then immersed in FJ (0.001% FJ/0.1% acetic acid) for 30 min.

For assessment of cell replication in islets, animals received two daily injections of 5-BrdU (50 mg/kg) for 3 days and were perfused with 4% paraformaldehyde 1 day after the last injection. Occurrence of dividing cells was determined by immunostaining with an antibody recognizing 5-BrdU (1:20, Dako, Copenhagen, Denmark) in 10 μm cryostat sections. The total number of cells containing 5-BrdU-positive nuclei per islet was assessed (a total number of 300 islets/genotype, and five different animals per genotype were analyzed).

Islet number and β-cell volume were determined in an unbiased procedure, according to the principles of stereological morphometry. To this end, serial sections were prepared, and immunostained for insulin (9003), using the peroxidase–anti-peroxidase method as described (50). Islet numbers were determined by counting all islets in every 6th section of the whole pancreas. Total β-cell volume was determined in serial sections using Image Promaster (measuring the area of 400 islets/genotype, three different animals per genotype). The investigator was unaware of the identity of the sections during analysis.

Electron microscopy

Small pieces of pancreatic tissue was fixed in a mixture of 1% glutaraldehyde and 3% paraformaldehyde in phosphate buffer, rinsed and postfixed for 1 h with 1% OsO_4, dehydrated in acetone and embedded in Polybed 812. Ultrathin sections

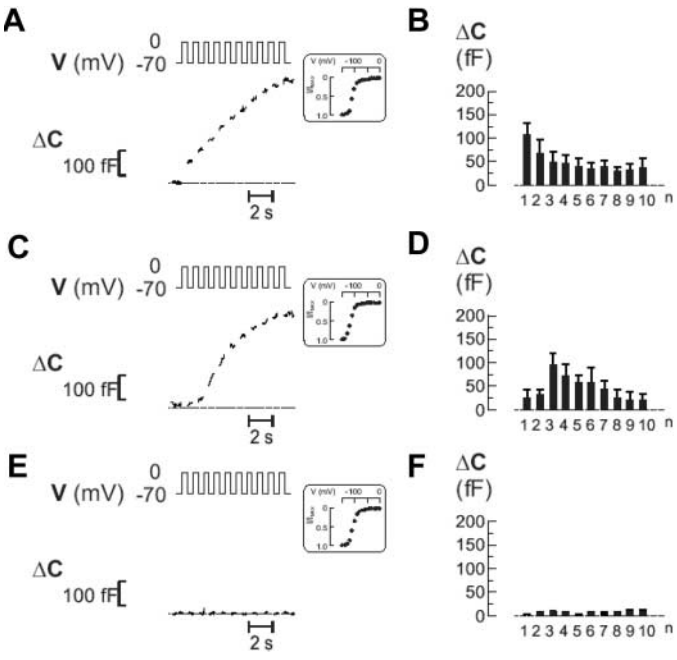

Figure 9. Depolarization-evoked exocytosis in single β-cells from control and R6/2 mice. (**A**) Exocytosis was evoked by trains of 10 depolarizations (V) and monitored as increases in cell capacitance (ΔC) in a control β-cell. Inset shows the voltage-dependent inactivation of the membrane Na^+ current at membrane potentials <-70 mV, typical of β-cells. (**B**) ΔC was evoked by the respective depolarizations in the train stimulus. Data are mean ± SEM in 13 control β-cells. (**C** and **D**), as in (A and B), but data was obtained in 11 8-week-old R6/2 beta-cells. (**E** and **F**), as in (A and B), but data was obtained in seven 12-week-old R6/2 beta-cells.

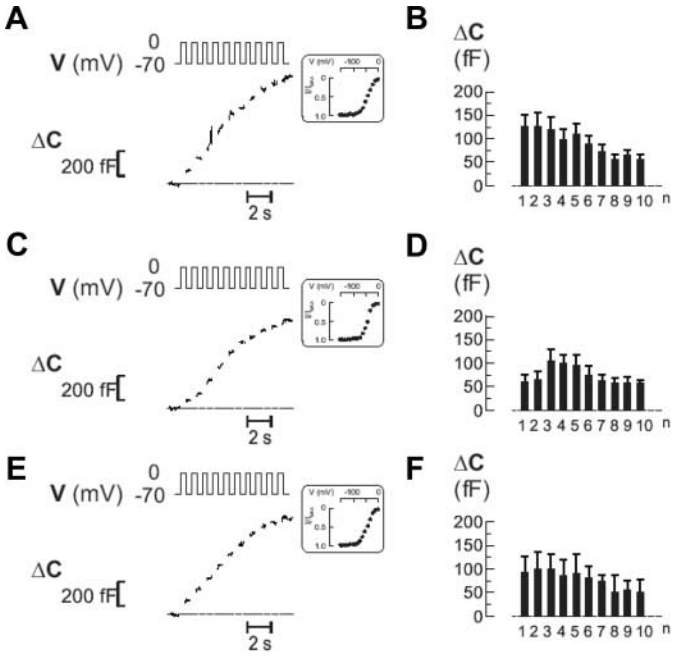

Figure 10. Single α-cell exocytosis in control and R6/2 mice. (**A**) Exocytosis was evoked by trains of 10 depolarizations (V) and monitored as increases in cell capacitance (ΔC) in a control α-cell. Inset shows the voltage-dependent inactivation of the membrane Na^+ current at membrane potentials within the membrane potential range physiologically relevant for islet cells (i.e. -70 to ~ 0 mV), used for identifying the α-cells. (**B**) ΔC was evoked by the respective depolarizations in the train stimulus. Data are mean ± SEM in four control α-cells. (**C** and **D**), as in (A and B), but data was obtained in seven 8-week-old R6/2 α-cells. (**E** and **F**), as in (A and B), but data was obtained in three 12-week-old R6/2 α-cells.

were cut and placed on copper grids before contrasted with 0.5% lead citrate and 4% uranyl acetate. Specimens were examined in a Philips CM10 transmission electron microscope.

Electrophysiology

The measurements were conducted using an EPC-10 patch-clamp amplifier in conjunction with the Pulse software suite (version 8.53; HEKA Elektronik, Lambrecht/Pfalz, Germany). The experiments were made using the standard whole-cell configuration of the patch-clamp technique, in which the cytosol is replaced by the pipette solution consisting of (in mM) 125 Cs-glutamate, 10 CsCl, 10 NaCl, 1 $MgCl_2$, 5 HEPES, 3 Mg-ATP, 0.1 cAMP and 0.05 EGTA (pH 7.2 with CsOH). Exocytosis was monitored as increases in cell capacitance using the sine+DC mode of the lock-in amplifier included in the Pulse software suite and was elicted by trains of ten 500 ms voltage-clamp depolarizations. Whole-cell Ca^{2+} current relationships were determined by 100 ms depolarizations going from the resting -70 mV to -50 mV and then in 10 mV increments up to $+50$ mV.

The identity of the islet cells was determined by measuring the voltage-dependence of Na^+ channel inactivation. This protocol consisted of a 50 ms prepulse to potentials between -150 mV and 0 mV, immediately followed by stepping the membrane potential to -10 mV where Na^+ current amplitudes were measured. In the figure insets, the Na^+ current amplitudes are expressed as fractions of the maximal current amplitude, and cells lacking Na^+ currents at membrane potentials relevant for β-cell electrical activity (i.e. between the resting membrane potential -70 mV and the peak of the β-cell action potential -10 mV) were identified as β-cells, whereas cells in which Na^+ channel inactivation occurs at more positive membrane potentials predominantly represent glucagon-releasing α-cells (51).

The extracellular bath solution contained (in mM) 118 NaCl, 20 TEA-Cl, 5.6 KCl, 2.6 $CaCl_2$, 1.2 $MgCl_2$, 5 glucose (unless otherwise indicated) and 5 HEPES (pH 7.4 with NaOH). The K^+ channel blocker TEA-Cl was used to block voltage-gated K^+-currents that otherwise obscured the considerably smaller voltage-gated Ca^{2+}-currents. The bath ($\sim$1.5 ml) was continuously perfused (6 ml/min) and the temperature maintained at $\sim 34^\circ$C. All electrophysiological data are given as average values ± SEM. Responses in 8- and 12-weeks-old control mice were identical and are pooled.

Statistical analysis

Mean ± SEM are given. All data were analyzed using a two-tailed unpaired *t*-test or two factor analysis of variance (ANOVA) when appropriate. $P < 0.05$ was considered statistically significant.

ACKNOWLEDGEMENTS

We are grateful to Ann-Helen Thorén, Britt-Marie Nilsson, Doris Persson and Elsy Ling for excellent technical assistance. M.B. and H.M. are supported by the Cure HD Initiative. H.M. is supported by the Swedish Research Council. E.R. is supported by the Swedish Research Council and the Diabetes Programme at Lund University. Å.P. is supported by the Swedish Brain Foundation. J.G. has a fellowship from the Foundation for Science and Technology (FCT, Portugal; SFRH/BD/6068/2001). P.B. is supported by the Swedish Research Council and the Hereditary Disease Foundation. N.P. is sponsored by Biodegradable controlled drug delivery systems for the treatment of brain diseases (BCDDS), QLRT-2000-02226, RTD-EU-Project, Quality of Life and Management of Living Resources. F.S. is supported by the Swedish Research Council, Novo Nordisk foundation and Påhlsson foundation. Å.P., N.P., J.Y.L. and P.B. are members of The European Union concerted action consortium 'Early pathogenetic markers for Slow Neurodegenerative Diseases' (EPSND, QLK6-CT-2000-00384) and would like to acknowledge the helpful discussions that have taken place within this network.

REFERENCES

1. Podolsky, S., Leopold N.A. and Sax D.S. (1972) Increased frequency of diabetes mellitus in patients with Huntington's chorea. *Lancet*, **24**, 1356–1358.
2. The Huntington's Disease Collaboration Group. (1993) A novel gene containing a trinucleotide repeat that is expanded and unstable on Huntington's disease chromosomes. *Cell*, **26**, 971–983.
3. Gutekunst, C.A., Levey, A.I., Heilman, C.J., Whaley, W.L., Yi, H., Nash, N.R., Rees, H.D., Madden, J.J. and Hersch, S.M. (1995) Identification and localization of huntingtin in brain and human lymphoblastoid cell lines with anti-fusion protein antibodies. *Proc. Natl Acad. Sci. USA*, **92**, 8710–8714.
4. Li, H., Li, S.H., Cheng, A.L., Mangiarini, L., Bates, G.P. and Li, X.J. (1999) Ultrastructural localization and progressive formation of neuropil aggregates in Huntington's disease transgenic mice. *Hum. Mol. Genet.*, **8**, 1227–1236.
5. Gauthier, L.R., Charrin, B.C., Borrell-Pages, M., Dompierre, J.P., Rangone, H., Cordelieres, F.P., De Mey, J., MacDonald, M.E., Lessmann, V., Humbert, S. and Saudou, F. (2004) Huntingtin controls neurotrophic support and survival of neurons by enhancing BDNF vesicular transport along microtubules. *Cell*, **118**,127–138.
6. Rigamonti, D., Bauer, J.H., De-Fraja, C., Conti, L., Sipione, S., Sciorati, C., Clementi, E., Hackam, A., Hayden, M.R., Li, Y. *et al.* (2000) Wild-type huntingtin protects from apoptosis upstream of caspase-3. *J. Neurosci.* **20**, 3705–3713.
7. Rigamonti, D., Sipione, S., Goffredo, D., Zuccato, C., Fossale, E. and Cattaneo, E. (2001) Huntingtin's neuroprotective activity occurs via inhibition of procaspase-9 processing. *J. Biol. Chem.* **276**, 14545–14548.
8. Gervais, F.G., Singaraja, R., Xanthoudakis, S., Gutekunst, C.A., Leavitt, B.R., Metzler, M., Hackam, A.S., Tam, J., Vaillancourt, J.P., Houtzager, V. *et al.* (2002) Recruitment and activation of caspase-8 by the Huntingtin-interacting protein Hip-1 and a novel partner Hippi. *Nat. Cell Biol.* **4**, 95–105.
9. Leavitt, B.R., Guttman, J.A., Hodgson, J.G., Kimel, G.H., Singaraja, R., Vogl, A.W. and Hayden, M.R. (2001) Wild-type huntingtin reduces the cellular toxicity of mutant huntingtin *in vivo*. *Am. J. Hum. Genet.* **68**, 313–324.
10. Ho, L.W., Brown, R., Maxwell, M., Wyttenbach, A. and Rubinsztein, D.C. (2001) Wild type Huntingtin reduces the cellular toxicity of mutant Huntingtin in mammalian cell models of Huntington's disease. *J. Med. Genet.* **38**, 450–452.
11. Zoghbi, H.Y. and Orr, H.T. (2000) Glutamine repeats and neurodegeneration. *Annu. Rev. Neurosci.*, **23**, 217–247.
12. DiFiglia, M., Sapp, E., Chase, K.O., Davies, S.W., Bates, G.P., Vonsattel, J.P. and Aronin, N. (1997) Aggregation of huntingtin in neuronal intranuclear inclusions and dystrophic neurites in brain. *Science*, **26**, 1990–1993.
13. Davies, S.W., Turmaine, M., Cozens, B.A., DiFiglia, M., Sharp, A.H., Ross, C.A., Scherzinger, E., Wanker, E.E., Mangiarini, L. and Bates, G.P. (1997) Formation of neuronal intranuclear inclusions underlies the neurological dysfunction in mice transgenic for the HD mutation. *Cell*, **90**, 537–548.
14. Sathasivam, K., Hobbs, C., Turmaine, M., Mangiarini, L., Mahal, A., Bertaux, F., Wanker, E.E., Doherty, P., Davies, S.W. and Bates, G.P. (1999) Formation of polyglutamine inclusions in non-CNS tissue. *Hum. Mol. Genet.*, **8**, 813–822.
15. Schilling, G., Becher, M.W., Sharp, A.H., Jinnah, H.A., Duan, K., Kotzuk, J.A., Slunt, H.H., Ratovitski, T., Cooper, J.K., Jenkins, N.A. *et al.* (1999) Intranuclear inclusions and neuritic aggregates in transgenic mice expressing a mutant N-terminal fragment of huntingtin. *Hum. Mol. Genet.*, **8**, 397–407.
16. Jenkins, B.G., Koroshetz, W.J., Beal, M.F. and Rosen, B.R. (1993) Evidence for impairment of energy metabolism *in vivo* in Huntington's disease using localized 1H NMR spectroscopy. *Neurology*, **43**, 2689–2695.
17. Beal, M.F. (1995) Aging, energy, and oxidative stress in neurodegenerative diseases. *Ann. Neurol.*, **38**, 357–366.
18. Nakao, N. and Brundin, P. (1998) Neurodegeneration and glutamate induced oxidative stress. *Prog. Brain. Res.*, **116**, 245–263.
19. Schilling, G., Sharp, A.H., Loev, S.J., Wagster, M.V., Li, S.H., Stine, O.C. and Ross, C.A. (1995) Expression of the Huntington's disease (IT15) protein product in HD patients. *Hum. Mol. Genet.*,**4**, 1365–1371.
20. Mangiarini, L., Sathasivam, K., Mahal, A., Mott, R., Seller, M. and Bates, G.P. (1997) Instability of highly expanded CAG repeats in mice transgenic for the Huntington's disease mutation. *Nat. Genet.*, **15**, 197–200.
21. Mangiarini, L., Sathasivam, K., Seller, M., Cozens, B., Harper, A., Hetherington, C., Lawton, M., Trottier, Y., Lehrach, H., Davies, S.W. and Bates, G.P. (1996) Exon 1 of the HD gene with an expanded CAG repeat is sufficient to cause a progressive neurological phenotype in transgenic mice. *Cell*, **87**, 493–506.
22. Murphy, K.P., Carter, R.J., Lione, L.A., Mangiarini, L., Mahal, A., Bates, G.P., Dunnett, S.B. and Morton, A.J. (2000) Abnormal synaptic plasticity and impaired spatial cognition in mice transgenic for exon 1 of the human Huntington's disease mutation. . *Neuroscience*, **20**, 5115–5123.
23. Petersén, Å., Gil, J., Maat-Schieman, Björkqvist, M., Tanila, H., Araújo, I.M., Smith, R., Popovic, N., Wierup, N., Norlén, P. *et al.* (2005) Orexin loss in Huntington's disease. *Hum. Mol. Genet.*, **14**, 1–9.
24. Turmaine, M., Raza, A., Mahal, A., Mangiarini, L., Bates, G.P. and Davies, S.W. (2000) Nonapoptotic neurodegeneration in a transgenic mouse model of Huntington's disease. *Proc. Natl Acad. Sci. USA*, **97**, 8093–8097.
25. Iannicola, C., Moreno, S., Oliverio, S., Nardacci, R., Ciofi-Luzzatto, A. and Piacentini, M. (2000) Early alterations in gene expression and cell morphology in a mouse model of Huntington's disease. *J. Neurochem.*, **75**, 830–839.
26. Helmlinger, D., Yvert, G., Picaud, S., Merienne, K., Sahel, J., Mandel, J.L. and Devys, D. (2002) Progressive retinal degeneration and dysfunction in R6 Huntington's disease mice. *Hum. Mol. Genet.*, **15**, 3351–3359.
27. Hurlbert, M.S., Zhou, W., Wasmeier, C., Kaddis, F.G., Hutton, J.C. and Freed, C.R. (1999) Mice transgenic for an expanded CAG repeat in the Huntington's disease gene develop diabetes. *Diabetes*, **48**, 649–651.
28. Luesse, H.G., Schiefer, J., Spruenken, A., Puls, C., Block, F. and Kosinski, C.M. (2001) Evaluation of R6/2 HD transgenic mice for therapeutic studies in Huntington's disease: behavioral testing and impact of diabetes mellitus. *Behav. Brain Res.*, **126**, 185–195.
29. Andreassen, O.A., Dedeoglu, A., Stanojevic, V., Hughes, D.B., Browne, S.E., Leech, C.A., Ferrante, R.J., Habener, J.F., Beal, M.F. and Thomas, M.K. (2002) Huntington's disease of the endocrine pancreas: insulin deficiency and diabetes mellitus due to impaired insulin gene expression. *Neurobiol. Dis.*, **11**, 410–424.
30. Schmued, L.C., Albertson, C. and Slikker, W. (1997) Fluoro-Jade: a novel fluorochrome for the sensitive and reliable histochemical localization of neuronal degeneration. *Brain Res.*, **751**, 37–46.

31. Gisselsson, D., Jonson, T., Petersén, Å., Strömbeck, B., Dal Cin. P., Höglund. M., Mittelman, F., Mertens, F. and Mandahl, N. (2001) Telomere dysfunction triggers extensive DNA fragmentation and evolution of complex chromosome abnormalities in human malignant tumors. *Proc. Natl Acad. Sci. USA*, **98**, 12683–12688.
32. Renström, E., Eliasson, L., Bokvist, K. and Rorsman, P. (1996) Cooling inhibits exocytosis in single mouse pancreatic B-cells by suppression of granule mobilization. *J. Physiol.*, **494**, 41–52.
33. Wiser, O., Trus, M., Hernandez, A., Renström, E., Barg, S., Rorsman, P. and Atlas, D. (1999) The voltage sensitive Lc-type Ca2+ channel is functionally coupled to the exocytotic machinery. *Proc. Natl Acad. Sci. USA*, **96**, 248–253.
34. Schulla, V., Renström, E., Feil, R., Feil, S., Franklin, I., Gjinovci, A., Jing, X.J., Laux, D., Lundquist, I., Magnuson, M.A. *et al.* (2003) Impaired insulin secretion and glucose tolerance in beta cell-selective Ca(v)1.2 Ca2+ channel null mice. *EMBO J.*, **22**, 3844–3854.
35. Kremer, H.P., Roos, R.A., Frolich, M., Radder, J.K., Nieuwenhuijzen Kruseman, A.C., Van der Velde, A. and Buruma, O.J. (1989) Endocrine functions in Huntington's disease. A two-and-a-half years follow-up study. *J. Neurol. Sci.*, **90**, 335–344.
36. Craft, S. and Watson, G.S. (2004) Insulin and neurodegenerative disorders. *Lancet Neurol.*, **3**, 169–178.
37. Ristow, M. (2004) Neurodegenerative disorders associated with diabetes mellitus. *J Mol. Med.*, **82**, 510–529.
38. Jenkins, B.G., Klivenyi, P., Kustermann, E., Andreassen, O.A., Ferrante, R.J., Rosen, B.R. and Beal, M.F. (2000) Nonlinear decrease over time in *N*-acetyl aspartate levels in the absence of neuronal loss and increases in glutamine and glucose in transgenic Huntington's disease mice. *J. Neurochem.*, **74**, 2108–2119.
39. Duan, W., Guo, Z., Jiang, H., Ware, M., Li, X.J. and Mattson, M.P. (2003) Dietary restriction normalizes glucose metabolism and BDNF levels, slows disease progression, and increases survival in huntingtin mutant mice. *Proc. Natl Acad. Sci. USA*, **100**, 2911–2916.
40. De Krijger, R.R., Aanstoot, H.J., Kranenburg, G., Reinhard, M., Visser, W.J. and Bruining, G.J. (1992) The midgestational human fetal pancreas contains cells coexpressing islet hormones. *Dev. Biol.*, **153**, 368–375.
41. Samols, E. and Stagner, J.I. (1990) Islet somatostatin—microvascular, paracrine, and pulsatile regulation. *Metabolism*, **39**, 55–60.
42. Butler, A.E., Janson, J., Soeller, W.C. and Butler, P.C. (2003) Increased beta-cell apoptosis prevents adaptive increase in beta-cell mass in mouse model of type 2 diabetes: evidence for role of islet amyloid formation rather than direct action of amyloid. *Diabetes*, **52**, 2304–2314.
43. Gil, J.M., Leist, M., Popovic, N., Brundin, P. and Petersen, A. (2004) Asialoerythropoetin is not effective in the R6/2 line of Huntington's disease mice. *BMC Neurosci.*, **10**, 5–17.
44. Lazic, S.E., Grote, H., Armstrong, R.J., Blakemore, C., Hannan, A.J., van Dellen, A. and Barker, R.A. (2004) Decreased hippocampal cell proliferation in R6/1 Huntington's mice. *Neuroreport*, **15**, 811–813.
45. Sathasivam, K., Woodman, B., Mahal, A., Bertaux, F., Wanker, E.E., Shima, D.T. and Bates, G.P. (2001) Centrosome disorganization in fibroblast cultures derived from R6/2 Huntington's disease (HD) transgenic mice and HD patients. *Hum. Mol. Genet.*, **10**, 2425–2435.
46. Weir, G.C., Laybutt, D.R., Kaneto, H., Bonner-Weir, S. and Sharma, A. (2001) Beta-cell adaptation and decompensation during the progression of diabetes. *Diabetes*, **50**, S154–S159.
47. Edwardson, J.M., Wang, C.T., Gong, B., Wyttenbach, A., Bai, J., Jackson, M.B., Chapman, E.R. and Morton, A.J. (2003) Expression of mutant huntingtin blocks exocytosis in PC12 cells by depletion of complexin II. *J. Biol. Chem.*, **278**, 30849–30853.
48. Hansson, O., Petersén, Å., Leist, M., Nicotera, P., Castilho, R.F. and Brundin, P. (1999) Transgenic mice expressing a Huntington's disease mutation are resistant to quinolinic acid-induced striatal excitotoxicity. *Proc. Natl Acad. Sci. USA*, **96**, 8727–8732.
49. Hohmeier, H.E., Mulder, H., Chen, G., Henkel-Rieger, R., Prentki, M. and Newgard, C.B. (2000) Isolation of INS-1-derived cell lines with robust ATP-sensitive K+ channel-dependent and -independent glucose-stimulated insulin secretion. *Diabetes*, **49**, 424–430.
50. Mulder, H., Lindh, A.C. and Sundler, F. (1993) Islet amyloid polypeptide gene expression in the endocrine pancreas of the rat: a combined *in situ* hybridization and immunocytochemical study. *Cell Tissue Res.*, **274**, 467–474.
51. Barg, S., Galvanovskis, J., Göpel, S.O., Rorsman, P. and Eliasson, L. (2000) Tight coupling between electrical activity and exocytosis in mouse glucagon-secreting alpha-cells. *Diabetes*, **49**, 1500–1510.